Multi-Frequency Co-Prime Arrays for High-Resolution Direction-of-Arrival Estimation

Elie BouDaher, *Student Member*, *IEEE*, Yong Jia, Fauzia Ahmad, *Senior Member*, *IEEE*, and Moeness G. Amin, *Fellow*, *IEEE*

Abstract - **This paper presents multi-frequency operation for increasing the number of resolvable sources in high-resolution direction-of-arrival (DOA) estimation using co-prime arrays. A single-frequency operation requires complicated and involved matrix completion to utilize the full extent of the degrees of freedom (DOFs) offered by the co-prime configuration. This processing complexity is attributed to the missing elements in the corresponding difference coarray. Alternate single-frequency schemes avoid such complexity by utilizing only the filled part of the coarray and, thus, cannot exploit all of the DOFs for DOA estimation. We utilize multiple frequencies to fill the missing coarray elements, thereby enabling the co-prime array to effectively utilize all of the offered DOFs. The sources are assumed to have a sufficient bandwidth to cover all the required operational frequencies. We consider both cases of sources with proportional and nonproportional power spectra at the employed frequencies. The former permits the use of multi-frequency measurements at the co-prime array to construct a virtual covariance matrix corresponding to a filled uniformly spaced coarray at a single frequency. This virtual covariance matrix can be employed for DOA estimation. The nonproportionality of the source spectra casts a more challenging situation, as it is not amenable to producing the same effect as that of an equivalent single-frequency filled coarray. Performance evaluation of the multi-frequency approach based on computer simulations is provided under both cases of proportional and nonproportional source spectra.**

This work was supported by the Office of Naval Research under grant N00014-13-1-0061.

E. BouDaher, F. Ahmad, and M. Amin are with the Center for Advanced Communications, College of Engineering, Villanova University, Villanova, PA, USA (e-mail: eboudahe@villanova.edu; fauzia.ahmad@villanova.edu; moeness.amin@villanova.edu).

Y. Jia was with the School of Electronic Engineering, University of Electronic Science and Technology of China, Chengdu, China. He is now with the College of Information Science and Technology, Chengdu, China (email: jiayong2014@cdut.edu.cn).

Index Terms — Co-prime arrays, DOA estimation, coarray, multiple frequencies, augmented matrices.

I. INTRODUCTION

Nonuniform linear arrays provide the ability to estimate the direction-of-arrival (DOA) of more sources than the number of physical sensors [1]-[6]. Recently, a new structure of nonuniform linear arrays, known as co-prime arrays, has been proposed [7], [8]. A co-prime configuration comprises two undersampled uniformly spaced subarrays with co-prime spatial sampling rates. Co-prime configurations have many advantages over other popular nonuniform configurations, including minimum redundancy arrays (MRA) [9], minimum hole arrays (MHA) [10], and nested arrays [11]. For a given number of physical sensors, MRAs and MHAs require an exhaustive search through all possible combinations of the sensors to find the optimal design [12], [13]. On the other hand, the positions of the sensors constituting the co-prime configuration have closed-form expressions. Although the same is true of nested arrays, the elements of one of the subarrays constituting the nested structure are closely separated, which may lead to problems due to mutual coupling between the sensors. Co-prime arrays reduce the mutual coupling between most adjacent sensors by spacing them farther apart [7]. Because of all of the aforementioned characteristics, co-prime arrays are finding broad applications in the areas of communications, radar, and sonar [14]-[20].

Similar to other nonuniform arrays, high-resolution DOA estimation with co-prime arrays can be performed using two main approaches. The first approach employs covariance matrix augmentation [21]-[23], while the second method vectorizes the data covariance matrix to emulate observations at a virtual array whose elements are given by the difference coarray (the set of all spatial lags generated by the physical array [24]) [8], [11]. Since the difference coarray of a co-prime array contains multiple missing elements or ‘holes’, the latter approach employs only that part of the difference coarray which has contiguous elements with no holes. As such, only a subset of the total degrees of freedom (DOFs) offered by the co-prime structure can be utilized for high-resolution DOA estimation using the vectorized covariance matrix approach. The augmented covariance matrix approach, on the other hand, can exploit all the DOFs but at the expense of additional complicated matrix completion processing [23].

In this paper, we consider multi-frequency operation to utilize all of the DOFs for DOA estimation in co-prime arrays. More specifically, a set of additional frequencies is employed to recover the missing lags through dilations of the coarray [25]. The sources are assumed to have a bandwidth large enough to cover all specific frequencies required for filling the holes. Only the array elements involved in filling the missing holes in the difference coarray are required to be operated at one or more of the additional frequencies. The multi-frequency measurements are used to construct a virtual covariance matrix corresponding to an equivalent filled uniformly spaced coarray at a single frequency [26]. High-resolution subspace techniques, such as MUSIC [27], can then be applied to this virtual covariance matrix for DOA estimation. It is important to note that full utilization of the DOFs using multiple additional frequencies comes with a restriction on the sources' spectra. More specifically, the source spectra at all operational frequencies are required to be proportional. Deviations from this restriction can lead to higher DOA estimation errors.

Multiple frequencies have previously been used for alias-free DOA estimation of broadband sources [28], [29]. In [28], frequency diversity was exploited on a single spatial sampling interval to mitigate spatial aliasing in DOA estimation with a sparse nonuniformly spaced array. Ambiguities in the source location estimates were resolved by proper choice of chosen operational frequencies in [29] for arrays with periodic spatial spectra. Spatial sampling interval diversity at a single narrowband frequency was exploited in [7] to disambiguate aliased DOAs. Both spatial sampling and frequency diversity were exploited in [26] through multi-frequency coarray augmentation for high-resolution DOA estimation. However, no attempt was made therein to select the best number of employed frequencies or determine their best values. We effectively apply the multi-frequency coarray augmentation to co-prime arrays in this paper. Our main contribution lies in exploiting the specific structure of the coarray corresponding to co-prime configuration to determine the number and values of the additional frequencies required for recovering the missing lags. We provide closed-form expressions for the additional frequencies, which are 'best' in the sense of minimum operational bandwidth requirements. We also describe when and how the redundancy in the coarray can be exploited to reduce the system hardware complexity for multi-frequency co-prime arrays. Further, we investigate the effects of noise and deviation from the proportional source spectra constraint on the DOA estimation performance of the multi-frequency co-prime arrays.

The remainder of the paper is organized as follows. The single-frequency based high-resolution DOA estimation using co-prime arrays is reviewed in Section II. In Section III, we describe the multi-frequency approach for filling the missing elements in the coarray and utilizing all the DOFs offered by the co-prime configuration for DOA estimation. Section IV delineates the system bandwidth requirement for the multi-frequency operation, taking into account the specificities of the coarray structure corresponding to co-prime arrays. Coarray redundancy is also examined to reduce the number of antennas engaging in multiple frequency operation. In Section V, performance of the proposed method is evaluated through extensive simulations under both proportional and nonproportional source spectra and Section VI concludes the paper.

II. High-Resolution DOA Estimation Using Single-Frequency Co-prime Arrays

A co-prime array consists of two undersampled uniform linear subarrays, one having M sensors positioned at $\{Nmd_0,\ 0 \leq m \leq M-1\}$, and the other comprising N sensors with positions $\{Mnd_0,\ 0 \leq n \leq N-1\}$ [11], M and N being co-prime integers and d_0 equal to one-half wavelength at the operating frequency ω_0. Without loss of generality, we assume $M < N$. With the two subarrays sharing the element at location 0, the co-prime array has a total of $M+N-1$ physical sensors. The element positions of the corresponding difference coarray form the set

$$S_0 = \{\pm(Mnd_0 - Nmd_0)\},\ 0 \leq n \leq N-1,\quad 0 \leq m \leq M-1, \tag{1}$$

which extends from $-N(M-1)d_0$ to $N(M-1)d_0$, but only the elements from $-(M+N-1)d_0$ and $(M+N-1)d_0$ are contiguous. As such, high-resolution schemes, such as MUSIC, can estimate only up to $M+N-1$ sources.

An extended co-prime configuration was proposed in [8], wherein the number of elements in the subarray with fewer sensors were doubled, as depicted in Fig. 1. The difference coarray of this configuration, shown in Fig. 2, extends from $-(2M-1)Nd_0$ to $(2M-1)Nd_0$, and has a contiguous set of elements between $-(MN+M-1)d_0$ and $(MN+M-1)d_0$. Thus, high-resolution DOA estimation can be performed to estimate $(MN+M-1)$ sources using the extended co-prime configuration. We will consider the extended co-prime configuration with $M < N$ in the remainder of this paper.

Assume that D sources with powers $\sigma_1^2(\omega_0), \sigma_2^2(\omega_0), \ldots, \sigma_D^2(\omega_0)$ impinge on the extended

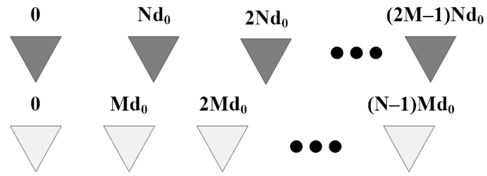

Figure 1. Extended co-prime array configuration.

co-prime array from directions $[\theta_1, \theta_2, \ldots, \theta_D]$ where θ is measured relative to broadside. The received data vector at frequency ω_0 can be expressed as

$$\mathbf{x}(\omega_0) = \mathbf{A}(\omega_0)\mathbf{s}(\omega_0) + \mathbf{n}(\omega_0), \tag{2}$$

where $\mathbf{s}(\omega_0) = [s_1(\omega_0)\ s_2(\omega_0)\ \ldots\ s_D(\omega_0)]^T$ is the source signal vector at ω_0, $\mathbf{n}(\omega_0)$ is the corresponding noise vector, $\mathbf{A}(\omega_0)$ is the array manifold matrix at ω_0, and the superscript $(.)^T$ denotes matrix transpose. The (i,j)th element of the array manifold can be expressed as

$$[\mathbf{A}(\omega_0)]_{i,j} = e^{jk_0 x_i \sin(\theta_j)}, i = 1, \ldots, 2M+N-1, \quad j = 1,2,\ldots,D \tag{3}$$

where x_i is the location of the ith physical sensor of the array, θ_j is the DOA of the jth source, and $k_0 = \omega_0/c$ is the wavenumber at ω_0 with c being the speed of propagation in free space. Assuming that the sources are uncorrelated and the noise is spatially and temporally white, the covariance matrix is obtained as

$$\begin{aligned}\mathbf{R}_{xx}(\omega_0) &= E\{\mathbf{x}(\omega_0)\mathbf{x}^H(\omega_0)\} \\ &= \mathbf{A}(\omega_0)\mathbf{R}_{ss}(\omega_0)\mathbf{A}^H(\omega_0) \\ &+ \sigma_n^2(\omega_0)\mathbf{I},\end{aligned} \tag{4}$$

where $\mathbf{R}_{ss}(\omega_0) = diag([\sigma_1^2(\omega_0)\ \sigma_2^2(\omega_0)\ \ldots\ \sigma_D^2(\omega_0)])$ is the source covariance matrix, $\sigma_n^2(\omega_0)$ is the noise variance**,** $\mathbf{I}$ is an identity matrix, the superscript $(\cdot)^H$ denotes Hermitian operation, and $E\{.\}$ denotes the statistical expectation operator. In practice, (4) is replaced by a sample average.

After forming the covariance matrix, two approaches can be employed to perform high-resolution DOA estimation. The first approach uses covariance matrix augmentation [21]-[23]. Following [22], since the difference coarray is filled between $-(MN+M-1)d_0$ and $(MN+M-1)d_0$, a virtual covariance matrix corresponding to an equivalent $(MN+M)$-element filled ULA can be formed by collecting specific elements of the estimated spatial covariance matrix $\mathbf{R}_{xx}(\omega_0)$ into a Toeplitz matrix. The resulting augmented covariance matrix may not always be positive definite and, thus, requires positive definite Toeplitz completion [22]. Subspace-based high-resolution methods can then be applied to the augmented covariance matrix for estimating up to $(MN+M-1)$ sources. The number of resolvable sources can be increased to $(2M-1)N$ by considering a partially specified virtual covariance matrix corresponding to an equivalent $(2M-1)N$+1-element filled ULA [23]. However, this comes at the expense of increased computational complexity due to a complicated and involved matrix completion process.

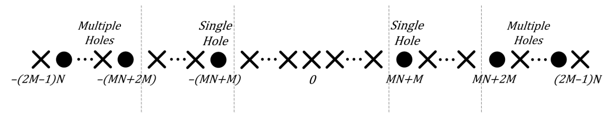

Figure 2. Difference coarray of the extended co-prime array.

The second approach vectorizes the covariance matrix $\mathbf{R}_{xx}(\omega_0)$ as [7]

$$\begin{aligned}\mathbf{z}(\omega_0) &= vec\big(\mathbf{R}_{xx}(\omega_0)\big) \\ &= \widetilde{\mathbf{A}}(\omega_0)[\sigma_1^2(\omega_0)\ \sigma_2^2(\omega_0)\ \ldots\ \sigma_D^2(\omega_0)]^T \\ &+ \sigma_n^2(\omega_0)\tilde{\mathbf{\imath}},\end{aligned} \tag{5}$$

where $\widetilde{\mathbf{A}}(\omega_0) = \mathbf{A}^*(\omega_0) \odot \mathbf{A}(\omega_0)$, the symbol '$\odot$' denotes the Khatri-Rao product, the superscript '*' denotes complex conjugation, and $\tilde{\boldsymbol{\imath}}$ is the vectorized form of $\mathbf{I}$. The vector $\boldsymbol{z}(\omega_0)$ acts as the received signal vector of a longer array whose elements positions are given by the difference coarray. However, as the sources are replaced by their powers, the model in (5) is similar to that of a fully coherent source environment. Spatial smoothing can be used to decorrelate the sources [8], [30], provided that only the filled part of the difference coarray between $-(MN+M-1)d_0$ and $(MN+M-1)d_0$ is employed. As such, the rank of the smoothed covariance matrix is equal to $(MN+M)$ [8], [11], which allows a maximum of $(MN+M-1)$ sources to be estimated by applying high-resolution techniques.

III. High Resolution DOA Estimation With Multi-frequency Co-prime Arrays

In this section, we describe how dual and multiple frequencies can be utilized to fill the holes in the coarray, thereby permitting the exploitation of the full DOFs that the co-prime configuration has to offer. The sources are assumed to have a bandwidth large enough to cover all frequencies required for filling the holes. Discrete Fourier transform (DFT) or filterbanks are used to decompose the array output vector into multiple non-overlapping narrowband components and extract the received signal at each considered frequency [31], [32]. The observation time is assumed to be sufficiently long to resolve the different frequencies.

Consider the extended co-prime configuration of Fig. 1, where the unit spacing d_0 is assumed to be half-wavelength at the reference frequency ω_0. The received signal at ω_0 is the same as in (2), whereas that obtained by operating the physical co-prime array at a different frequency, $\omega_q = \alpha_q \omega_0$, has the form

$$\mathbf{x}(\omega_q) = \mathbf{A}(\omega_q)\mathbf{s}(\omega_q) + \mathbf{n}(\omega_q), \quad (6)$$

where $\mathbf{A}(\omega_q)$ is the $(2M+N-1) \times D$ array manifold at ω_q with its (i,j)th element given by

$$[\mathbf{A}(\omega_q)]_{i,j} = e^{jk_q x_i \sin(\theta_j)}. \quad (7)$$

In (7), $k_q = \omega_q/c$ is the wavenumber at ω_q. Since $k_q = \alpha_q k_0$, (7) can be rewritten as

$$[\mathbf{A}(\omega_q)]_{i,j} = e^{jk_0 \alpha_q x_i \sin(\theta_j)}. \quad (8)$$

Comparing (3) and (8), we observe that the array manifold at ω_q is equivalent to the array manifold at ω_0 of a scaled version of the physical co-prime array. The position of the ith element in the equivalent scaled array is given by $\alpha_q x_i$. This results in the difference coarray at ω_q to be a scaled version of the coarray at the reference frequency ω_0 [33]. Values of ω_q higher than ω_0 cause an expansion of the coarray, while the coarray contracts if ω_q is lower than ω_0. In other words, operation at the additional frequency adds extra points at specific locations in the coarray. A suitable choice of additional operating frequencies will cause some of these extra points to occur at the locations of the holes in the difference coarray at ω_0.

A. Virtual Covariance Matrix Formation

Let the total number of operational frequencies, including the reference, be Q. As shown below, a virtual covariance matrix can be constructed using the multi-frequency measurements, which is equivalent to that of a ULA with $(2M-1)N+1$ elements operating at the reference frequency [26], [34]. This would allow DOA estimation of $(2M-1)N$ sources instead of $(MN+M-1)$ sources using $(2M+N-1)$ physical sensors of the co-prime array.

A $(2M+N-1) \times (2M+N-1)$ support matrix $\mathbf{C}(\omega_q)$ is defined such that its (i,j)th element is given by [26], [34]

$$[\mathbf{C}(\omega_q)]_{i,j} = \alpha_q x_i - \alpha_q x_j. \quad (9)$$

That is, the (i,j)th element of $\mathbf{C}(\omega_q)$ is the spatial lag or the coarray element position which is the support of the (i,j)th element of the covariance matrix $\mathbf{R}_{xx}(\omega_q)$

$$\begin{aligned}\mathbf{R}_{xx}(\omega_q) = E\left\{\mathbf{x}(\omega_q)\mathbf{x}(\omega_q)^H\right\} \\ = \mathbf{A}(\omega_q)\mathbf{R}_{ss}(\omega_q)\mathbf{A}^H(\omega_q) \\ + \sigma_n^2(\omega_q)\mathbf{I},\end{aligned} \quad (10)$$

where $\mathbf{R}_{ss}(\omega_q) = diag([\sigma_1^2(\omega_q)\ \sigma_2^2(\omega_q) \ldots \sigma_D^2(\omega_q)])$ is the source covariance matrix at frequency ω_q. It should be noted that $\mathbf{C}(\omega_q) = \alpha_q \mathbf{C}(\omega_0)$, where $\mathbf{C}(\omega_0)$ is the support matrix at the reference frequency ω_0. Let $\mathbf{C}_v(\omega_0)$ and $\mathbf{R}_v(\omega_0)$ be the support and the covariance matrices corresponding to the desired ULA with $(2M-1)N+1$ sensors operating at ω_0. Given that the Q operational frequencies are sufficient to fill all the holes in the difference coarray of the co-prime array, then

$$[\mathbf{C}_v(\omega_0)]_{i,j} = [\mathbf{C}(\omega_q)]_{p,r}, \text{ for some } q, p, r, \text{ and all } i \text{ and } j \quad (11)$$

Let h be the map that arranges selected elements of the multi-frequency support matrices, $\{\mathbf{C}(\omega_q)\}_{q=0}^{Q-1}$, into the desired virtual support matrix $\mathbf{C}_v(\omega_0)$. Using the same map, the virtual covariance matrix $\mathbf{R}_v(\omega_0)$ corresponding to the equivalent ULA can then be constructed from the covariance matrices $\{\mathbf{R}_{xx}(\omega_q)\}_{q=0}^{Q-1}$ corresponding to the Q operational frequencies [26].

For illustration, we consider a co-prime array with $M=2$ and $N=3$. The sensor positions of the two uniform linear subarrays are given by $[0, 2d_0, 4d_0]$ and $[3d_0, 6d_0, 9d_0]$, respectively. The support matrix $\mathbf{C}(\omega_0)$ at the reference frequency takes the form

$$\mathbf{C}(\omega_0) = \begin{bmatrix} 0 & -2 & -3 & -4 & -6 & -9 \\ 2 & 0 & -1 & -2 & -4 & -7 \\ 3 & 1 & 0 & -1 & -3 & -6 \\ 4 & 2 & 1 & 0 & -2 & -5 \\ 6 & 4 & 3 & 2 & 0 & -3 \\ 9 & 7 & 6 & 5 & 3 & 0 \end{bmatrix} d_0. \quad (12)$$

The difference coarray of this configuration is shown in Fig. 3. It has holes at $-8d_0$ and $8d_0$. In order to fill these holes and form the virtual covariance matrix, an additional frequency $\omega_1 = 8/9\omega_0$ is required. With this choice of the second operational frequency, the support matrix at ω_1 is given by

$$\mathbf{C}(\omega_1) = \begin{bmatrix} 0 & -\frac{16}{9} & -\frac{8}{3} & -\frac{32}{9} & -\frac{16}{3} & -8 \\ \frac{16}{9} & 0 & -\frac{8}{9} & -\frac{16}{9} & -\frac{32}{9} & -\frac{56}{9} \\ \frac{8}{3} & \frac{8}{9} & 0 & -\frac{8}{9} & -\frac{8}{3} & -\frac{16}{3} \\ \frac{32}{9} & \frac{16}{9} & \frac{8}{9} & 0 & -\frac{16}{9} & -\frac{40}{9} \\ \frac{16}{3} & \frac{32}{9} & \frac{8}{3} & \frac{16}{9} & 0 & -\frac{8}{3} \\ 8 & \frac{56}{9} & \frac{16}{3} & \frac{40}{9} & \frac{8}{3} & 0 \end{bmatrix} d_0. \quad (13)$$

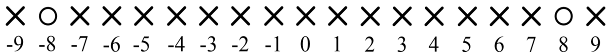

Figure 3. Difference coarray at the reference frequency $\boldsymbol{\omega_0}$ for M = 2, N = 3.

The support matrix $\mathbf{C}_v(\omega_0)$ of the desired 10-element ULA, whose elements are positioned at $[0, 1, \dots, 9]d_0$, has the structure

$$\mathbf{C}_v(\omega_0) = \begin{bmatrix} 0 & -1 & -2 & \dots & -8 & -9 \\ 1 & 0 & -1 & \dots & -7 & -8 \\ 2 & 1 & 0 & \dots & -6 & -7 \\ \vdots & \vdots & \vdots & \ddots & \vdots & \vdots \\ 8 & 7 & 6 & \dots & 0 & -1 \\ 9 & 8 & 7 & \dots & 1 & 0 \end{bmatrix}. \quad (14)$$

From (12)-(14), we observe that several possibilities exist for constructing $\mathbf{C}_v(\omega_0)$ using $\mathbf{C}(\omega_0)$ and $\mathbf{C}(\omega_1)$, since several elements of $\mathbf{C}(\omega_0)$ and $\mathbf{C}(\omega_1)$ correspond to the same element of $\mathbf{C}_v(\omega_0)$. Either a single element or an average of all such elements can be used to specify the map for forming the desired virtual support matrix and, subsequently, the virtual covariance matrix $\mathbf{R}_v(\omega_0)$ [26], [34].

It should be noted that since the difference coarray at ω_0 has two holes at $\pm 8d_0$, only those elements of $\mathbf{R}_{xx}(\omega_1)$ that correspond to these two lags are required to form $\mathbf{R}_v(\omega_0)$. This means that instead of operating the entire co-prime array at ω_1, only the sensors that produce the $\pm 8d_0$ lags at ω_1 should be operated at the additional frequency. For example, operating the two sensors with positions $[0\ 9]d_0$ at ω_1 produces the following reduced support matrix

$$\begin{aligned} \mathbf{C}_r(\omega_1) = \frac{8}{9}\mathbf{C}_r(\omega_0) &= \frac{8}{9}\begin{bmatrix} 0 & -9 \\ 9 & 0 \end{bmatrix} d_0 \\ &= \begin{bmatrix} 0 & -8 \\ 8 & 0 \end{bmatrix} d_0. \end{aligned} \quad (15)$$

The two support matrices $\mathbf{C}(\omega_0)$ and $\mathbf{C}_r(\omega_1)$ can then be combined to form $\mathbf{C}_v(\omega_0)$. This procedure results in reducing hardware complexity. A more detailed discussion in this regard is provided in Section IV-D.

B. Proportional Spectra Requirement

For multi-frequency DOA estimation, the normalized covariance matrices are employed instead of $\{\mathbf{R}_{xx}(\omega_q)\}_{q=0}^{Q-1}$. The (i, j)th element of the normalized covariance matrix $\overline{\mathbf{R}}_{xx}(\omega_q)$ at frequency ω_q can be expressed as [34]

$$[\overline{\mathbf{R}}_{xx}(\omega_q)]_{i,j} = \frac{E\left\{[\mathbf{x}(\omega_q)]_i[\mathbf{x}^*(\omega_q)]_j\right\}}{\frac{1}{N_s(\omega_q)}E\{\mathbf{x}^H(\omega_q)\mathbf{x}(\omega_q)\}}, \quad (16)$$

where $[\mathbf{x}(\omega_q)]_i$ is the ith element of the data vector at frequency ω_q, and $N_s(\omega_q)$ is the number of sensors that are operated at ω_q. This results in the source and noise powers in the covariance matrix representation of (10) being replaced by the normalized powers [26], which are given by

$$\bar{\sigma}_k^2(\omega_q) = \frac{\sigma_k^2(\omega_q)}{\sum_{d=1}^{D} \sigma_d^2(\omega_q) + \sigma_n^2(\omega_q)} \quad (17)$$

$$\bar{\sigma}_n^2(\omega_q) = \frac{\sigma_n^2(\omega_q)}{\sum_{d=1}^{D} \sigma_d^2(\omega_q) + \sigma_n^2(\omega_q)} \quad (18)$$

where $\bar{\sigma}_k^2(\omega_q)$ is the normalized power of the kth source at frequency ω_q and $\bar{\sigma}_n^2(\omega_q)$ is the normalized noise power at the same frequency. The virtual covariance matrix $\mathbf{R}_v(\omega_0)$, constructed by using the normalized covariance matrices $\{\overline{\mathbf{R}}_{xx}(\omega_q)\}_{q=0}^{Q-1}$ following the procedure outlined in Section III.A, must appear to have been generated by the virtual array as if it were the actual array operating at frequency ω_0. However, some of the elements of the constructed virtual covariance matrix have contributions from frequencies other than ω_0. The virtual covariance matrix will be exact provided that the normalized power of each source is independent of frequency,

$$\bar{\sigma}_k^2(\omega_q) = \sigma_k^2, \text{ for all } q \in \{0, 1, \dots, Q-1\}, \text{ and all } k \in \{1, 2, \dots, D\} \quad (19)$$

For a high signal-to-noise ratio (SNR), a sufficient condition for the virtual covariance matrix to be exact is that the sources must have proportional spectra at the employed frequencies [34]. That is,

$$\frac{\sigma_k^2(\omega_q)}{\sigma_l^2(\omega_q)} = \beta_{k,l}, \quad (20)$$

where $\beta_{k,l}$ is a constant for each source pair (k, l) over all frequencies ω_q. This condition is satisfied, for example, when the D sources are BPSK or chirp-like signals.

IV. Frequency Selection For Multi-frequency Operation Using Extended Co-prime Arrays

In order to quantify the operational frequency set for filling the holes, we first need to examine the specific structure of the difference coarray corresponding to an extended co-prime configuration. Consider the difference coarray of Fig. 2, which corresponds to the co-prime array of Fig. 1. The total number of filled and missing elements in the coarray equals $2(2M-1)N+1$, whereas the total number of holes is determined to be $(M-1)(N-1)$. As the coarray is symmetric, we only focus on the portion corresponding to the non-negative lags. We observe that the portion of the coarray extending from 0 to $(MN + M - 1)d_0$ is uniform and has no holes. The first hole appears at $(MN + M)d_0$, followed by another filled part from $(MN + M + 1)d_0$ to $(MN + 2M - 1)d_0$. The final part of the coarray from $(MN + 2M)d_0$ to $(2M - 1)Nd_0$ is non-uniform and contains $((M - 1)(N - 1)/2) - 1$ holes.

A. One Additional Frequency (Dual-Frequency Operation)

The two holes at $-(MN + M)d_0$ and $(MN + M)d_0$ can be filled using only one additional frequency. The choice of the additional frequency is not unique. The value of ω_1 that minimizes the separation between ω_0 and ω_1 is given by

$$\omega_1 = \alpha_1 \omega_0 = \frac{MN + M}{MN + M + 1}\omega_0, \tag{21}$$

where the numerator and the denominator of the scaling factor α_1 correspond to the respective positions of the hole to be filled and the adjacent filled element to the right of the hole (considering the non-negative lags) that is used to fill it. Note that the value of ω_1 in (21) is less than ω_0. It can be readily shown that using neighboring elements other than the right adjacent one yields values of ω_1, which result in a larger separation from ω_0.

Filling the two holes at $\pm(MN + M)d_0$ causes the uniform part of the difference coarray to extend from $-(MN + 2M - 1)d_0$ to $(MN + 2M - 1)d_0$. As a result, up to $(MN + 2M - 1)$ sources can be estimated after forming the corresponding virtual covariance matrix. This implies that, compared to the single frequency operation, M additional sources can be estimated using one extra frequency in addition to ω_0.

B. Multiple Additional Frequencies (Multiple Frequency Operations)

The remaining $(M - 1)(N - 1) - 2$ holes in the difference coarray can also be filled through the use of additional frequencies. The exact number and values of the frequencies are tied to the non-uniformity pattern in the coarray beyond $\pm(MN + 2M)d_0$, which varies from one co-prime configuration to the other. Assuming that each additional frequency is used to fill only two holes (one missing positive element and its negative counterpart), we require at the most $\frac{1}{2}((M - 1)(N - 1) - 2) = (MN - M - N)/2$ additional frequencies to yield a filled uniform coarray extending from $-(2M - 1)Nd_0$ to $(2M - 1)Nd_0$.

C. Maximum Frequency Separation

The maximum frequency separation from the reference frequency determines the required operational bandwidth of the antennas and receiver front end for the proposed multi-frequency approach. It is determined by the distance of the farthest hole from its nearest filled right neighbor and the location of the neighbor. The maximum number of consecutive holes in the difference coarray is $(M - 1)$ and this pattern of $(M - 1)$ consecutive holes repeats $\lfloor N/M \rfloor$ times at each end of the difference coarray, as shown in Fig. 4 for the non-negative lags. However, it is the first set of $(M - 1)$ consecutive holes (those on extreme left in Fig. 4) that requires operational frequencies with the maximum separation from ω_0 in order to be filled. The repeated hole patterns at larger lags yield smaller frequency separation values. The first missing element in the leftmost set of consecutive holes occurs at $\left[(2M - 1)N - (M - 1) - \left(\left\lfloor \frac{N}{M} \right\rfloor - 1\right) M\right] d_0$, while the nearest right filled element is positioned at $\left[(2M - 1)N - \left(\left\lfloor \frac{N}{M} \right\rfloor - 1\right) M\right] d_0$. Therefore, the required frequency to fill this hole is given by

$$\tilde{\omega} = \frac{(2M - 1)N - (M - 1) - \left(\left\lfloor \frac{N}{M} \right\rfloor - 1\right) M}{(2M - 1)N - \left(\left\lfloor \frac{N}{M} \right\rfloor - 1\right) M}\omega_0 \tag{22}$$

The maximum frequency separation can, thus, be computed as

$$\begin{aligned}\Delta\omega_{max} &= |\omega_0 - \tilde{\omega}| \\ &= \left| \frac{1 - M}{(2M - 1)N - \left(\left\lfloor \frac{N}{M} \right\rfloor - 1\right) M} \right| \omega_0.\end{aligned} \tag{23}$$

Table I shows the maximum frequency separation for different co-prime array configurations under two cases: i) when one additional frequency is used to fill the first pair of holes, and ii) when all holes are filled using multiple frequencies. For each of the aforementioned cases, the additional number of estimated sources compared to single frequency operation are also specified in Table I. We observe that the maximum frequency separation decreases with increasing values of M and N. This is because both the holes and the elements that are used to fill them occur at larger spatial lags for higher values of M and N, which, in turn, implies a smaller value of the scaling factor in (23).

D. Reduced Hardware Complexity

Since only a few observations at each employed frequency other than ω_0 are used for the proposed multi-frequency high-resolution DOA estimation scheme and the remaining observations are discarded, it is not economical to operate the entire physical array at each of the additional $Q - 1$ frequencies. Therefore, only the receive elements that generate the desired spatial lags for filling the holes need to be operating at more than one frequency. As determined in Section

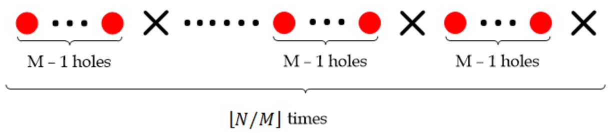

Figure 4. Positive end part of the difference coarray corresponding to the co-prime array.

IV.C, the bandwidth requirement for the multi-frequency operation is not that high, especially for larger values of M and N. As such, only the multi-frequency receive elements require a DFT or a filterbank to extract the information at the different frequencies, leading to a significant reduction in system hardware complexity.

It becomes of interest to determine the smallest number of sensors that are required to operate at the additional frequency or frequencies. As the holes occur in symmetric pairs, the lags corresponding to each pair can be generated using only two sensors in the physical array. In case of redundancy in the difference coarray, there is more than one antenna pair that can generate the same spatial lag. In order to reduce the number of antennas engaging in multiple frequency processing, one should therefore seek and identify each sensor that participates in filling all the holes or at least many of them. This becomes important when there is flexibility in sensor participation choices implied by the redundancy property of the spatial lags. Clearly, only the redundant spatial lags occurring beyond the first symmetric hole pair at $\pm(MN+M)d_0$ need to be considered, since these are used to fill the holes in the difference coarray. It can be readily shown that there are a total of $2(M-2)$ redundant lags beyond $\pm(MN+M)d_0$ at $\pm(MN+kN)d_0$ with weights given by

$$W(\pm(MN+kN)d_0) = M-k, \quad \text{for } k = 1,2,\ldots,M-2. \tag{24}$$

For illustration, we consider an example where $M=4$ and $N=5$. The co-prime array consists of 12 elements positioned at $[0\ 4\ 5\ 8\ 10\ 12\ 15\ 16\ 20\ 25\ 30\ 35]d_0$. Fig. 5 shows the difference coarray weighting function corresponding to this array. The first hole pair in the coarray occurs at $\pm(MN+M)d_0 = \pm 24d_0$. Beyond the first holes, $2(M-2)=4$ redundant lags exist. The first redundant lag pair occurs at $\pm(MN+N)d_0 = \pm 25d_0$ with weight equal to $(M-1)=3$. The second redundant pair occurs at $\pm(MN+2N)d_0 = \pm 30d_0$ and has a weight of $(M-2)=2$. In order to minimize the maximum frequency separation, only the redundant lags that occur immediately to the right of the holes (considering the nonnegative lags) can be used. For the case where $mod(N,M)=1$, all the redundant lags in the nonuniform part of the coarray occur immediately after the holes. This can be confirmed by observing the weighting function in Fig. 5. For the case where $mod(N,M)=M-1$, none of the redundant lags are immediately to the right of the holes, as illustrated in Fig. 6 for the case where $M=4$ and $N=7$. For the remaining cases, only a subset of the redundant lags in the nonuniform part is immediately after the holes.

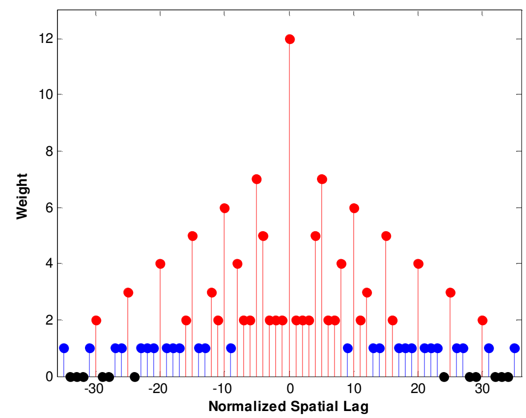

Figure 5. Difference coarray weight function: $M = 4$, $N = 5$.

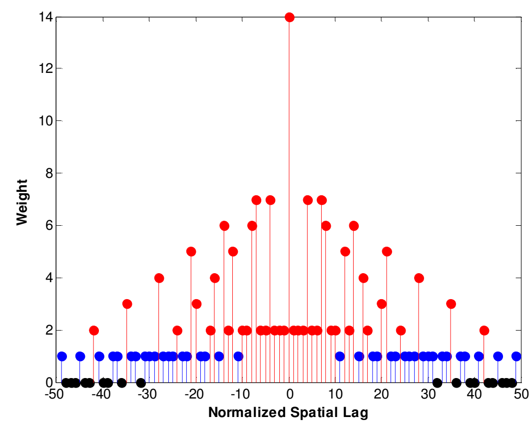

Figure 6. Difference coarray weight function: $M = 4$, $N = 7$.

For the illustration of the role of redundancy in reducing sensor engagement in hole filling, we provide the following two examples. Table II shows the additional frequencies and the corresponding sensor pairs that are required to fill all nine holes in the difference coarray for the case where $M=4$ and $N=7$. The corresponding physical array consists of 14 sensors at $[0\ 4\ 7\ 8\ 12\ 14\ 16\ 20\ 21\ 24\ 28\ 35\ 42\ 49]d_0$. It is clear from Table II that only the 6 sensors located at $[0\ 4\ 8\ 12\ 16\ 49]d_0$ are required to operate at more than one frequency in order to fill all the holes in the coarray. It should be noted that since $mod(N,M)=M-1$ in this example, the redundant lags in the

TABLE II

REQUIRED FREQUENCIES AND SENSOR PAIRS, $M = 4, N = 7$

Frequencies	Holes	Sensor Pairs
$\omega_1 = (32/33)\omega_0$	$\pm 32d_0$	$[16\ 49]d_0$
$\omega_2 = (36/37)\omega_0$	$\pm 36d_0$	$[12\ 49]d_0$
$\omega_3 = (39/41)\omega_0$	$\pm 39d_0$	$[8\ 49]d_0$
$\omega_4 = (40/41)\omega_0$	$\pm 40d_0$	$[8\ 49]d_0$
$\omega_5 = (43/45)\omega_0$	$\pm 43d_0$	$[4\ 49]d_0$
$\omega_6 = (44/45)\omega_0$	$\pm 44d_0$	$[4\ 49]d_0$
$\omega_7 = (46/49)\omega_0$	$\pm 46d_0$	$[0\ 49]d_0$
$\omega_8 = (47/49)\omega_0$	$\pm 47d_0$	$[0\ 49]d_0$
$\omega_9 = (48/49)\omega_0$	$\pm 48d_0$	$[0\ 49]d_0$

difference coarray cannot be used to further decrease the number of antennas that would operate at more than one frequency. Table III shows the required frequencies and the corresponding sensor pairs for the case where $M = 4$ and $N = 5$. Since $mod(N, M) = 1$, different sensor pairs can be used to fill the same holes. As shown in Table III, the pairs that include common sensors at different frequencies are chosen in order to minimize the number of sensors that operate at more than one frequency. Table IV shows the percentage of sensors that need to be operated at more than one frequency for different co-prime array configurations. We observe that the number of sensors that need to be operated at multiple frequencies has a lower bound of one-third of the total number of sensors in the array, which is achieved for co-prime configurations with $N = M + 1$. It should be noted that the same choice of $N = M + 1$ also minimizes the total number of sensors in the co-prime arrays, as demonstrated in [15].

V. NUMERICAL RESULTS

In this section, we present DOA estimation results based on the MUSIC algorithm using multi-frequency co-prime arrays. Both proportional and nonproportional source spectra cases are considered and performance comparison with single-frequency operation is provided. We employ the filled part of the coarray and covariance matrix augmentation for DOA estimation using MUSIC under single frequency operation. The root mean squared error (RMSE) in all examples in this section is based on a single realization, unless stated otherwise.

A. *Proportional Spectra*

We first consider a co-prime array configuration with six physical sensors, corresponding to $M = 2$ and $N = 3$. The first uniform linear subarray consists of three elements positioned at $[0, 2d_0, 4d_0]$ and the

TABLE IV

PERCENTAGE OF MULTI-FREQUENCY SENSORS FOR DIFFERENT CO-PRIME PAIRS

M	N	Multi-frequency sensors
2	3	$2/6 = 33.3\%$
3	4	$3/9 = 33.3\%$
3	5	$4/10 = 40.0\%$
4	5	$4/12 = 33.3\%$
4	7	$6/14 = 42.8\%$
5	7	$6/16 = 37.5\%$
6	7	$6/18 = 33.3\%$

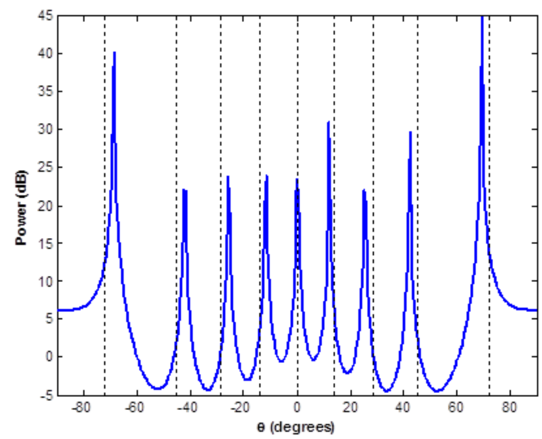

Figure 7. MUSIC spectrum using single frequency, $D = 9$ sources with proportional spectra.

second subarray has four elements with positions $[0, 3d_0, 6d_0, 9d_0]$, with d_0 equal to one-half wavelength at ω_0. The difference coarray of this configuration, shown in Fig. 3, has two holes at $\pm 8d_0$, which can be filled using an additional frequency $\omega_1 = (8/9)\omega_0$. We consider 9 sources with proportional spectra, where $\sigma_d^2(\omega_1) = 3\sigma_d^2(\omega_0)$ for $d = 0,1, \ldots, 8$. The sources are uniformly spaced between -0.95 and 0.95 in the reduced angular coordinate $\sin(\theta)$. A total of 2000 snapshots are used and the SNR is set to 0 dB for both frequencies. The estimated spatial spectrum, where only the reference frequency ω_0 is used, is provided in Fig. 7. The elements in the covariance matrix corresponding to the holes in the difference coarray have been filled with zeros. This is equivalent to the case where the sources have zero powers at the additional frequency. The vertical lines in the figure indicate the true DOAs of the sources. We observe from Fig. 7 that the single frequency approach fails to correctly estimate the DOAs of most of the targets. The RMSE is found to be 2.55°. This is expected since the considered co-prime

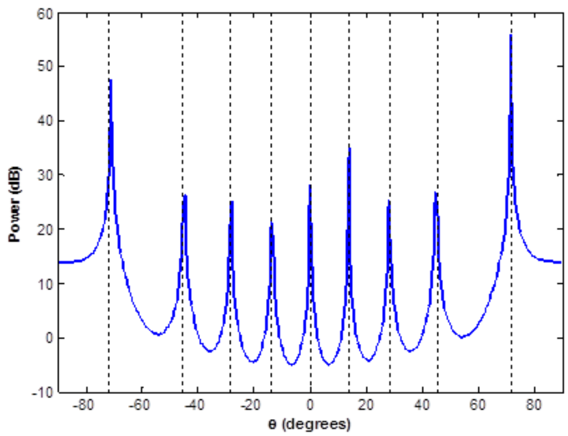

Figure 8. MUSIC spectrum using two frequencies, $D = 9$ sources with proportional spectra.

array operating at a single frequency can resolve a maximum of 7 sources. Fig. 8 depicts the estimated spatial spectrum using the dual-frequency approach. We can clearly see that the DOAs of all sources have been correctly estimated. In this case, the RMSE of the DOA estimates is equal to $0.67°$.

In the second example, we consider a co-prime configuration with $M = 5$ and $N = 7$. The 7 sensors of the first ULA are positioned at $[0, 5, 10, 15, 20, 25, 30]d_0$, and the second ULA has 10 elements with positions $[0, 7, 14, 21, 28, 35, 42, 49, 56, 63]d_0$. The corresponding coarray extends from $-63d_0$ to $63d_0$ and has a total of 24 holes. The uniform portion of the coarray only extends from $-39d_0$ to $39d_0$. Thus, the single frequency operation can resolve a maximum of 39 sources. One additional frequency $\omega_1 = (40/41)\omega_0$ is first used to fill the holes at $\pm 40d_0$ in the coarray. As a result, the uniform part of the coarray now includes the lags from $-44d_0$ to $44d_0$, thereby increasing the maximum number of resolvable sources from 39 to 44. We consider 44 sources with $\sin(\theta_d)$ uniformly distributed between -0.97 and 0.97. The sources are assumed to have identical power spectra at the two frequencies. A total of 2000 snapshots are considered and the SNR is set to 0 dB for both frequencies. Fig. 9 shows the estimated spatial spectrum, wherein the DOAs of all 44 sources have been accurately estimated. The RMSE is determined to be $0.31°$ in this case. Next, we employ 12 additional frequencies to fill all 24 holes in the coarray. The additional frequencies and the corresponding holes they fill are listed in Table V. It should be noted that the holes could have also been filled using only six additional frequencies. These frequencies are $\omega_1 = 5\omega_0$, $\omega_2 = 2\omega_0$ $\omega_3 = (47/49)\omega_0$, $\omega_4 = 3\omega_0$, $(\omega_5 = 59/63)\omega_0$, and $\omega_6 = (61/63)\omega_0$. However, this choice of frequencies results in a maximum frequency separation of $4\omega_0$, compared

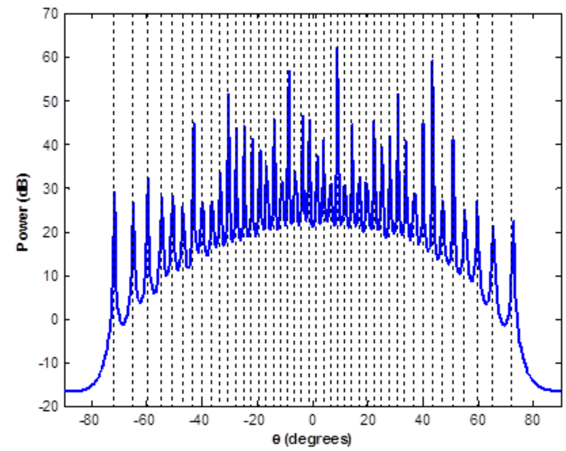

Figure 9. MUSIC spectrum with dual frequencies, $D = 44$ sources with proportional spectra.

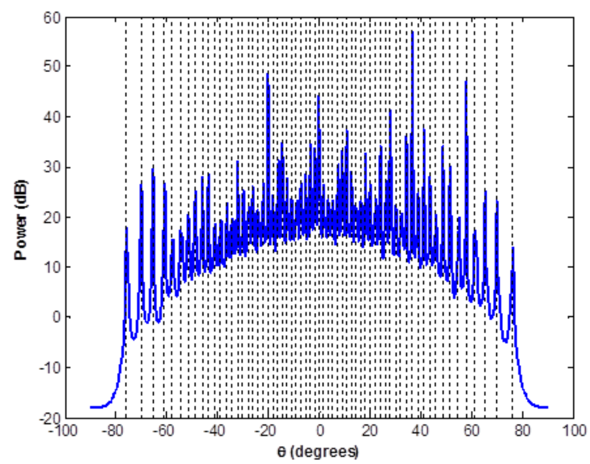

Figure 10. MUSIC spectrum with multiple frequencies, $D = 63$ sources with proportional spectra.

to $0.064\omega_0$ for the set of frequencies in Table V. Fig. 10 shows the estimated spatial spectrum corresponding to 63 sources with $\sin(\theta_d)$ uniformly distributed between -0.97 and 0.97 and equal power spectra at the 12 frequencies. The SNR and the number of snapshots are taken to be the same as for Fig. 9. Again, the multi-frequency approach has estimated all sources accurately and the RMSE is $0.2°$.

B. Nonproportional Spectra

We evaluate the DOA estimation performance of the multi-frequency co-prime arrays when the condition of proportional source spectra is violated. In the first example, we consider the same array and source configuration as in the first example in Section V.A with $M = 2$ and $N = 3$. However, the 9 sources are now assumed to have nonproportional spectra at ω_0 and $\omega_1 = (8/9)\omega_0$. More specifically, the source

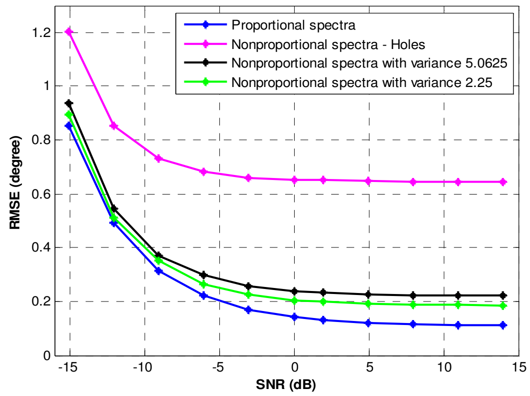

Figure 11. RMSE vs. SNR for $M = 2$, $N = 3$, $D = 9$.

powers at ω_0 are assumed to be identical and equal to unity, whereas the source powers associated with ω_1 are assumed to independently follow a truncated Gaussian distribution with a mean of 5.5 and a common variance. Two different values of 2.25 and 5.06 are considered for the variance. The variance controls the degree of non-proportionality. A higher variance increases the degree of non-proportionality of the source spectra, whereas a lower variance results in smaller variations in the source powers. Fig. 11 depicts the RMSE as a function of the variance and the SNR, averaged over 2000 Monte Carlo runs. For comparison, the RMSE corresponding to both single-frequency operation and dual-frequency operation for the case when the sources have proportional spectra are also included. As expected, the single-frequency approach, wherein the elements of the virtual covariance matrix corresponding to the holes in the coarray are filled with zeros, provides the worst performance. Further, the RMSE corresponding to the multi-frequency approach for nonproportional spectra increases with increasing variance. This results in a degradation of the estimation performance. Finally, the multi-frequency approach works best when the spectra are proportional and the SNR is higher.

In the following example, we compare the performance of the multi-frequency approach to single-frequency DOA estimation as a function of the assumed model order. The same array configuration with $M = 2$ and $N = 3$ is used. Two cases are considered in this example. The first case deals with sources with proportional spectra, while the second considers sources with nonproportional spectra. For the nonproportional case, the source powers associated with ω_0 are assumed to be identical and equal to unity, and the source powers associated with ω_1 follow a truncated Gaussian distribution with a mean of 5.5 and a variance 2. In both cases, the actual number of sources is set to 4, and the assumed model order is

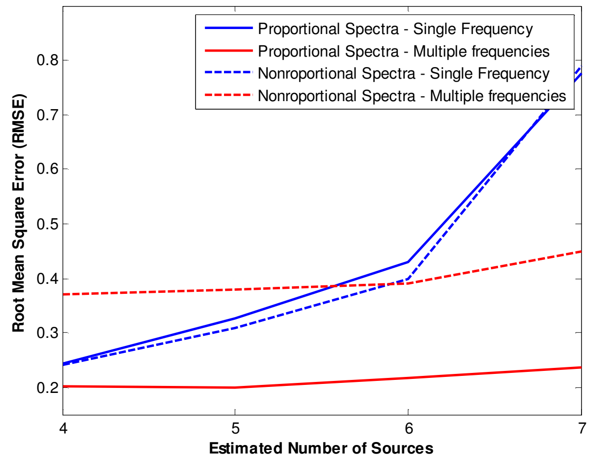

Figure 12. RMSE vs. Assumed Model Order for M = 2, N = 3, D = 4.

varied between 4 and 7. 1000 Monte Carlo are considered in this example. Fig. 12 shows the RMSE, averaged over 1000 Monte Carlo runs, as a function of the assumed model order for both cases. In computing the RMSE, only the detected peaks that are closest to the actual source directions were considered. From Fig. 12, we observe that, as expected, the performance of the single-frequency approach is not affected by the nonproportionality of the source spectra. On the other hand, the multi-frequency DOA estimation exhibits superior performance for sources with proportional spectra compared to those with nonproportional spectra. Further, the multi-frequency approach is less sensitive to errors in model order as compared to the single-frequency approach.

The effect of the degree of non-proportionality on DOA estimation performance is next examined for the co-prime configuration of the second example in Section V.A with $M = 5$ and $N = 7$ under both dual and multi-frequency operation. Again, the source powers at ω_0 are assumed to be all equal to unity, whereas the source powers at additional frequencies follow a truncated Gaussian distribution with a mean of 5.5 and a common variance. Fig. 13 provides the RMSE, averaged over 2000 Monte Carlo runs, as a function of SNR and variance under the dual-frequency operation for 44 sources. Similar observations to those in Fig. 11 can be made in this case as well. However, two differences can be noticed by comparing the RMSE plots in Figs. 11 and 13. First, the RMSE takes on lower values for all considered DOA estimation methods and variances for the co-prime configuration with $M = 5$ and $N = 7$. Second, the difference in performance between the single and dual frequency operations for the nonproportional spectra cases is much smaller at higher SNR values in this example. This is due to the

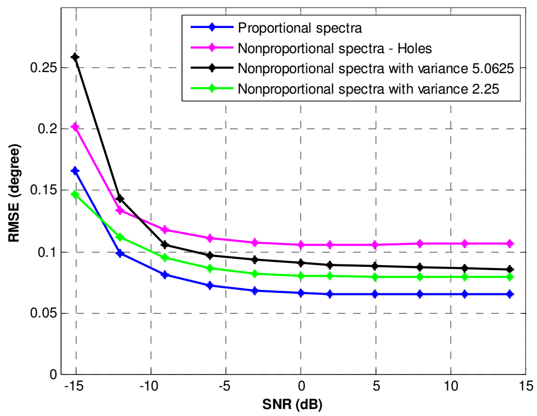

Figure 13. RMSE vs. SNR for $M = 5$, $N = 7$, $D = 44$.

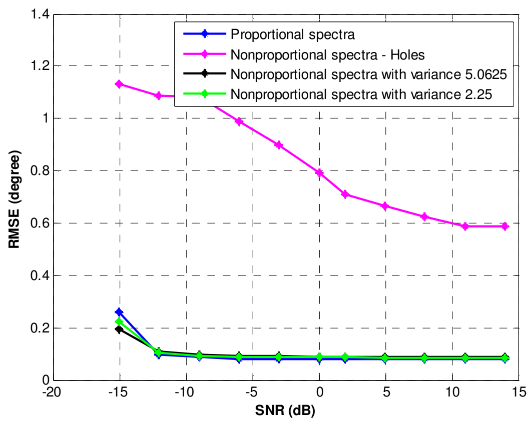

Figure 14. RMSE vs. SNR for $M = 5$, $N = 7$, $D = 60$.

fact that the ratio of the number of missing elements to the total number of elements in the filled part of the difference coarray is smaller in this example. This results in a smaller percentage of elements in the virtual covariance matrix to come from a different frequency or be filled with zeros for single frequency operation. The RMSE plots for the multi-frequency operation to fill all 24 holes are provided in Fig. 14, which corresponds to 60 sources with $\sin(\theta_d)$ uniformly distributed between -0.97 and 0.97. The performance difference between multi-frequency operation for sources with non-proportional spectra and those with proportional spectra is even less noticeable in this case, though the RMSE values themselves are slightly higher for high SNR. Also, the single-frequency operation exhibits a higher RMSE since a higher percentage of the virtual covariance matrix elements now have a zero value compared to that for Fig. 13.

The final example in this section examines the estimation performance for varying degree of nonproportionality of the source spectra for different

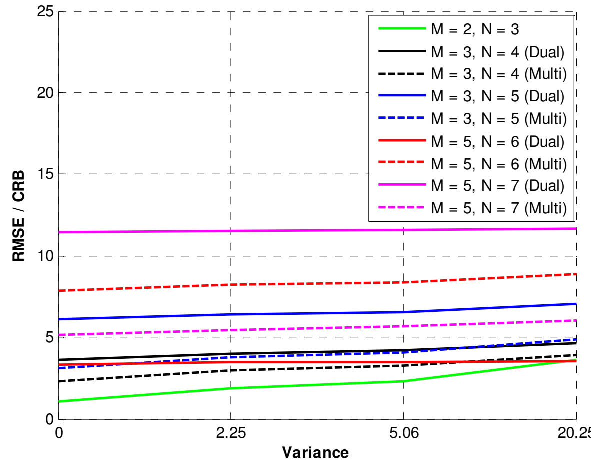

Figure 15. RMSE vs. variance, SNR = 0 dB.

values of M and N with the SNR fixed at 0 dB. Both dual-frequency operation for filling only the first hole pair and multi-frequency operation for filling all the holes are considered for each co-prime configuration. For each case, the maximum number of resolvable sources was used. A total of 2000 Monte Carlo runs were considered in this example. The source powers associated with the reference frequency ω_0 are identical and equal to unity. For the additional frequencies, the source powers follow a truncated Gaussian distribution with a mean of 5.5 and a common variance. The corresponding RMSE plots as a function of the variance of the source powers are depicted in Fig. 15. In order to have a fair comparison among co-prime arrays of different sizes, each RMSE plot is normalized by the Cramer Rao Bound (CRB) of an equivalent ULA with total number of elements equal to the number of contiguous nonnegative lags in the corresponding difference coarray. By examining Fig. 15, the following observations are in order. First, as expected, a decrease in the variance of the sources spectra results in a reduced estimation error. Second, by comparing the results of dual and multiple frequency operation for fixed M and N, we observe that, in general, the normalized RMSE error is smaller for the case when more than one additional frequencies are used.

C. Comparison with Sparse Reconstruction

Sparse reconstruction can be used in lieu of MUSIC for DOA estimation using multi-frequency co-prime arrays [35]. Unlike the proposed MUSIC-based approach, all of the lags generated by the multi-frequency operation, in addition to those that fill the holes in the difference coarray, can be utilized for DOA estimation using sparse reconstruction. This is because sparse reconstruction does not require the additional lags to fall on a uniform grid (integer multiples of the unit spacing). Utilization of all generated lags, in this case, enhances the number of DOFs for DOA estimation, leading to an increased number of resolvable sources. However, the performance of the sparse reconstruction approach is affected by the coherence of the data measurement operator. In addition, it is computationally more expensive than MUSIC.

In order to compare the performance of sparse reconstruction and MUSIC based multi-frequency approaches, we consider the following example. The same array configuration as in the first example in Section V.A is used. Two frequencies, ω_0 and $\omega_1 = (8/9)\omega_0$, are employed; the latter can fill the holes in the corresponding difference coarray so that the multi-frequency MUSIC technique can be applied. Nine sources with directions uniformly spaced between -0.9 and 0.9 in the reduced angular coordinate $\sin(\theta)$ are used, which is the maximum number of sources that can be resolved using the multi-frequency MUSIC approach. Two separate cases are considered in this example. The first case assumes sources with proportional spectra, while the second considers sources with nonproportional spectra. For the latter, the source powers at ω_0 are assumed to be identical and equal to unity, whereas the source powers associated with ω_1 are assumed to independently follow a truncated Gaussian distribution with a mean of 5.5 and a variance of 2. Fig. 16 shows the RMSE, averaged over 1000 Monte Carlo runs, as a function of the SNR for both cases. The SNR is assumed to be identical at both frequencies and is varied from -10 dB to 10 dB with a 2.5 dB increment. It can be readily observed that the multi-frequency MUSIC approach outperforms the sparse reconstruction method for all SNR values when the sources have proportional spectra. In case of sources with nonproportional spectra, the multi-frequency MUSIC method outperforms the sparse reconstruction approach for low values of SNR, whereas both methods achieve similar performance at high SNR values. For both proportional and nonproportional spectra cases, the sparse reconstruction approach exhibits significantly degraded performance at low SNR values. This is expected since the accuracy of the sparse reconstruction methods suffers in high noise cases.

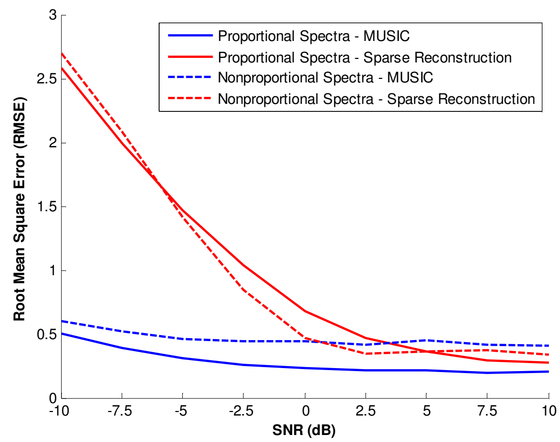

Figure 16. RMSE vs. SNR comparison between MUSIC and sparse reconstruction based multi-frequency approaches.

VI. Conclusion

A multi-frequency technique has been presented for high-resolution DOA estimation using co-prime arrays. A virtual covariance matrix at the reference frequency is created using elements of the narrowband covariance matrices corresponding to the different employed frequencies. The virtual covariance matrix corresponds to a uniform linear array with a difference coarray of the same extent as that of the co-prime array, except that the coarray of the ULA is filled whereas that of the co-prime array has holes. This permits the co-prime array to handle all of the degrees of freedom offered by the co-prime configuration. Observations and insights were provided with regards to i) the maximum frequency separation required to fill all the holes in the difference coarray, ii) the lower bound on the number of sensors required to operate at more than one frequency, and iii) the performance under non-proportional source spectra case. These insights contribute towards better understanding the offerings and limitations of the proposed multi-frequency approach. Supporting simulation examples were provided for DOA estimation of the proposed approach under both proportional and nonproportional spectra. The results demonstrated that the proposed approach can estimate DOAs with high accuracy for sources with proportional spectra, while for non-proportional spectra, the estimation error varies with the SNR as well as the values of M and N. The effect of nonproportionality was shown to be not as significant at high SNR for higher values of M and N as for lower values.

References

[1] S. Chandran, *Advances in Direction-of-Arrival Estimation*, Norwood, MA: Artech House, 2006.

[2] H. L. Van Trees, *Optimum Array Processing: Part IV of Detection, Estimation and Modulation Theory*, New York, NY: Wiley, 2002.

[3] T. E. Tuncer and B. Friedlander, *Classical and Modern Direction-of-Arrival Estimation*, Boston, MA: Academic Press (Elsevier), 2009.

[4] L. C. Godara, “Application of antenna arrays to mobile communications. II. Beam-forming and direction-of-arrival considerations,” *Proc. IEEE*, vol. 85, no. 8, pp. 1195–1245, 1997.

[5] R. A. Monzingo and T. W. Miller, *Introduction to Adaptive Arrays*, New York, NY: Wiley, 1980.

[6] D. H. Johnson and D. E. Dudgeon, *Array Signal Processing: Concepts and Techniques*, Englewood, NJ: Prentice Hall, 1993.

[7] P. P. Vaidyanathan and P. Pal, "Sparse sensing with co-prime samplers and arrays," *IEEE Trans. Signal Process.*, vol. 59, no. 2, pp. 573–586, 2011.

[8] P. Pal and P. P. Vaidyanathan, "Coprime sampling and the MUSIC algorithm," in *Proc. IEEE Digital Signal Process. Workshop and IEEE Signal Process. Education Workshop*, Sedona, AZ, 2011.

[9] A. Moffet, "Minimum-redundancy linear arrays," *IEEE Trans. Antennas Propag.*, vol. AP-16, no. 2, pp. 172–175, Mar. 1968.

[10] G. S. Bloom and S. W. Golomb, "Application of numbered undirected graphs," *Proc. IEEE*, vol. 65, no. 4, pp. 562–570, Apr. 1977.

[11] P. Pal and P. P. Vaidyanathan, "Nested arrays: a novel approach to array processing with enhanced degrees of freedom," *IEEE Trans. Signal Process.*, vol. 58, no. 8, pp. 4167–4181, Aug. 2010.

[12] J. C. P. Miller, "Difference bases, three problems in additive number theory," in A. D. L. Atkin and B. J. Birch (Eds.), *Computers in Number Theory*, pp. 299–322, London, UK: Academic Press, 1971.

[13] K. A. Blanton and J. H. McClellan, "New search algorithm for minimum redundancy linear arrays," in *Proc. IEEE Int. Conf. Acoustics, Speech, and Signal Process.,* vol.2, Apr. 1991, pp. 1361–1364.

[14] Q. Wu and Q. Liang, "Coprime sampling for nonstationary signal in radar signal processing," *EURASIP Journal on Wireless Communications and Networking* 2013, 2013:58.

[15] K. Adhikari, J. R. Buck, and K. E. Wage, "Beamforming with extended co-prime sensor arrays," in *Proc. IEEE Int. Conf. Acoustics, Speech and Signal Process.*, May 2013, pp. 4183-4186.

[16] Y. Zhang, M. Amin, F. Ahmad, and B. Himed, "DOA estimation using a sparse uniform linear array with two CW signals of co-prime frequencies," in *Proc. IEEE 5th Int. Workshop Computational Advances in Multi-Sensor Adaptive Process.*, Dec. 2013, pp. 404-407.

[17] Z. Tan and A. Nehorai, "Sparse direction of arrival estimation using co-prime arrays with off-grid targets," *IEEE Signal Process. Lett.,* vol. 21, no. 1, pp. 26-29, Jan. 2014.

[18] A. T. Pyzdek and R. L. Culver, "Processing methods for coprime arrays in complex shallow water environments," *J. Acoust. Soc. Am.*, vol. 135, no. 4, pp. 2392-2392, 2014.

[19] J. Chen and Q. Liang, "Rate distortion performance analysis of nested sampling and coprime sampling," *EURASIP Journal on Advances in Signal Process.* 2014, 2014:18.

[20] J. Ramirez, J. Odom, and J. Krolik, "Exploiting array motion for augmentation of co-prime arrays," in *Proc. IEEE 8th Int. Sensor Array and Multichannel Signal Process. Workshop,* Jun. 2014, pp. 525–528.

[21] S. U. Pillai, Y. Bar-Ness, and F. Haber, "A new approach to array geometry for improved spatial spectrum estimation," *Proc. IEEE*, vol. 73, pp. 1522–1524, Oct. 1985.

[22] Y. I. Abramovich, D. A. Gray, A. Y. Gorokhov, and N. K. Spencer, "Positive-definite Toeplitz completion in DOA estimation for nonuniform linear antenna arrays. I. Fully augmentable arrays," *IEEE Trans. Signal Process.*, vol. 46, pp. 2458–2471, Sep. 1998.

[23] Y. I. Abramovich, N. K. Spencer, and A. Y. Gorokhov, "Positive-definite Toeplitz completion in DOA estimation for nonuniform linear antenna arrays. II. Partially augmentable arrays," *IEEE Trans. Signal Process.*, vol. 47, pp. 1502–1521, Jun. 1999.

[24] R. T. Hoctor and S. A. Kassam, "The unifying role of the coarray in aperture synthesis for coherent and incoherent imaging," *Proc. IEEE*, vol. 78, no. 4, pp. 735–752, Apr. 1990.

[25] E. BouDaher, Y. Jia, F. Ahmad, and M. Amin, "Direction-of-arrival estimation using multi-frequency co-prime arrays," in *Proc. 22nd European Signal Process. Conf.*, Sep. 2014.

[26] J. L. Moulton, and S. A. Kassam, "Resolving more sources with multi-frequency coarrays in high-resolution direction-of-arrival estimation," in *Proc. 43rd Annual Conference on Information Sciences and Systems*, Mar. 2009, pp. 772–777.

[27] R. Schmidt, "Multiple emitter location and signal parameter estimation," *IEEE Trans. Antennas Propag.*, vol. 34, pp. 276–280, Mar. 1986.

[28] M. J. Hinich, "Processing spatially aliased arrays," *J. Acoust. Soc. Am.*, vol. 64, no. 3, pp. 793–795, 1978.

[29] M. G. Amin, "Sufficient conditions for aliased free direction of arrival estimation in periodic spatial spectra," *IEEE Transactions on Antennas and Propagation*, vol. 41, no. 4, pp. 508-511, April 1993.

[30] T. J. Shan, M. Wax, and T. Kailath, "On spatial smoothing for direction-of-arrival estimation of coherent signals," *IEEE Trans. Acoust., Speech, Signal Process.*, vol. 33, no. 4, pp. 806–811, Aug. 1985.

[31] Y. Yoon, L. M. Kaplan, and J. H. McClellan, "TOPS: New DOA estimator for wideband signals," *IEEE Trans. Signal Process.*, vol. 54, no. 6, pp. 1977-1989, Jun 2006.

[32] H. Wang and M. Kaveh, "Coherent signal-subspace processing for the detection and estimation of angles of arrival of multiple wide-band sources," *IEEE Trans. Acoust., Speech, Signal Processing*, vol. 33, no. 4, pp. 823–831, Mar 1985.

[33] F. Ahmad and S. A. Kassam, "Performance analysis and array design for wide-band beamformers," *Journal of Electronic Imaging*, vol. 7, no. 4, pp. 825-838, Oct. 1998.

[34] J. L. Moulton, "Enhanced high-resolution imaging through multiple-frequency coarray augmentation," Ph.D. dissertation, Electrical and Systems Engineering, University of Pennsylvania, Philadelphia, PA, 2010.

[35] E. BouDaher, F. Ahmad, and M. G. Amin, "Sparse reconstruction for direction-of-arrival estimation using multi-frequency co-prime arrays," *EURASIP Journal on Advances in Signal Processing,* 2014, pp. 2014:168.

TABLE I
MAXIMUM FREQUENCY SEPARATION FOR DUAL AND MULTI-FREQUENCY

M	N	Dual-frequency		Multi-frequency	
		Additional estimated sources	$\Delta\omega_{max}$	Additional estimated sources	$\Delta\omega_{max}$
2	3	2	11.11%	2	11.11%
3	4	3	6.25%	6	10.00%
3	5	3	5.26%	8	8.00%
5	7	5	2.44%	24	6.35%
7	9	7	1.41%	48	5.13%

TABLE III
REQUIRED FREQUENCIES AND SENSOR PAIRS, $M = 4, N = 5$

Frequencies	Holes	Sensor Pairs	Chosen Pairs
$\omega_1 = (24/25)\omega_0$	$\pm 24d_0$	$[0\ 25]d_0$, $[5\ 30]d_0$, $[10\ 35]d_0$,	$[0\ 25]d_0$
$\omega_2 = (28/30)\omega_0$	$\pm 28d_0$	$[0\ 30]d_0$, $[5\ 35]d_0$	$[0\ 30]d_0$
$\omega_3 = (29/30)\omega_0$	$\pm 29d_0$	$[0\ 30]d_0$, $[5\ 35]d_0$	$[0\ 30]d_0$
$\omega_4 = (32/35)\omega_0$	$\pm 32d_0$	$[0\ 35]d_0$	$[0\ 35]d_0$
$\omega_5 = (33/35)\omega_0$	$\pm 33d_0$	$[0\ 35]d_0$	$[0\ 35]d_0$
$\omega_6 = (34/35)\omega_0$	$\pm 34d_0$	$[0\ 35]d_0$	$[0\ 35]d_0$

TABLE V
ADDITIONAL FREQUENCIES AND CORRESPONDING HOLES, $M = 5, N = 7$

Frequency	Holes	Frequency	Holes
$\omega_1 = (40/41)\omega_0$	$\pm 40d_0$	$\omega_7 = (55/56)\omega_0$	$\pm 55d_0$
$\omega_2 = (45/46)\omega_0$	$\pm 45d_0$	$\omega_8 = (57/58)\omega_0$	$\pm 57d_0$
$\omega_3 = (47/48)\omega_0$	$\pm 47d_0$	$\omega_9 = (59/63)\omega_0$	$\pm 59d_0$
$\omega_4 = (50/51)\omega_0$	$\pm 50d_0$	$\omega_{10} = (60/63)\omega_0$	$\pm 60d_0$
$\omega_5 = (52/53)\omega_0$	$\pm 52d_0$	$\omega_{11} = (61/63)\omega_0$	$\pm 61d_0$
$\omega_6 = (54/56)\omega_0$	$\pm 54d_0$	$\omega_{12} = (62/63)\omega_0$	$\pm 62d_0$

Elie BouDaher (S'10) received the B.S. degree in Computer and Communications Engineering from the American University of Science and Technology, Beirut, Lebanon, in 2011, and the M.S. degree in Electrical Engineering from Villanova University, Villanova, PA, in 2013. He is currently pursuing the Ph.D. degree in the field of Signal Processing and Communications at Villanova University. His research interests include sparse reconstruction, sparse arrays signal processing, and electromagnetic modeling and optimization.

Yong Jia received the Ph.D. degree in Signal and Information Processing from University of Electronic Science and Technology of China, Chengdu, China, in 2014. He was a Visiting Researcher at the Center for Advanced Communications, Villanova University, Villanova, PA, from February to August in 2013. Currently, he is a lecturer with the Information Engineering at Chengdu University of Technology, Chengdu, China. His research interests include array signal processing, through-wall radar signal processing, and life-sign detection.

Fauzia Ahmad (SM'06) received her Ph.D. degree in Electrical Engineering from the University of Pennsylvania, Philadelphia, PA in 1997. Since 2002, she has been with the Villanova University, Villanova, PA, where she is currently a Research Professor with the Center for Advanced Communications in the College of Engineering, and is the Director of the Radar Imaging Laboratory. She is a Senior Member of the Institute of Electrical and Electronics Engineers (IEEE), 2006 and a Senior Member of the International Society for Optics and Photonics (SPIE), 2012. Her general research interests are in the areas of statistical signal and array processing, radar imaging, radar signal processing, compressive sensing, waveform diversity and design, target localization and tracking, direction finding, and ultrasound imaging. She has published more than 170 journal articles and peer-reviewed conference papers and 5 book chapters in the aforementioned areas.

Dr. Ahmad is an Associate Editor of the IEEE TRANSACTIONS ON SIGNAL PROCESSING. She also serves on the Editorial Boards of the IET Radar, Sonar & Navigation and the SPIE/IS&T Journal of Electronic Imaging. She is a member of the IEEE Aerospace and Electronic System Society's Radar Systems Panel. She also chairs the SPIE Conference Series on Compressive Sensing. Dr. Ahmad is the Lead Guest Editor of IEEE SIGNAL PROCESSING MAGAZINE March-2016 Special Issue on Signal Processing for Assisted Living. She was the Lead Guest Editor of the SPIE/IS&T Journal of Electronic Imaging April-June 2013 Special Section on Compressive Sensing for Imaging and the Lead Guest Editor of the IET Radar, Sonar & Navigation February-2015 Special Issue on Radar Applied to Remote Patient Monitoring and Eldercare.

Moeness G. Amin (F'01) received his Ph.D. degree in Electrical Engineering from University of Colorado in 1984. He has been on the Faculty of the Department of Electrical and Computer Engineering at Villanova University since 1985. In 2002, he became the Director of the Center for Advanced Communications, College of Engineering. He is a Fellow of the Institute of Electrical and Electronics Engineers (IEEE), 2001; Fellow of the International Society of Optical Engineering, 2007; and a Fellow of the Institute of Engineering and Technology (IET), 2010. Dr. Amin is a Recipient of the IEEE Third Millennium Medal, 2000; Recipient of the 2014 IEEE Signal Processing Society Technical Achievement Award; Recipient of the 2009 Individual Technical Achievement Award from the European Association of Signal Processing; Recipient of the 2010 NATO Scientific Achievement Award; Recipient of the Chief of Naval Research Challenge Award, 2010; Recipient of Villanova University Outstanding Faculty Research Award, 1997; and the Recipient of the IEEE Philadelphia Section Award, 1997. He was a Distinguished Lecturer of the IEEE Signal Processing Society, 2003-2004, and is currently the Chair of the Electrical Cluster of the Franklin Institute Committee on Science and the Arts. Dr. Amin has over 700 journal and conference publications in the areas of Wireless Communications, Time-Frequency Analysis, Sensor Array Processing, Waveform Design and Diversity, Interference Cancellation in Broadband Communication Platforms, satellite Navigations, Target Localization and Tracking, Direction Finding, Channel Diversity and Equalization, Ultrasound Imaging and Radar Signal Processing. He has co-authored 18 book chapters. He is the Editor of the two books *Through the Wall Radar Imaging* and *Compressive Sensing for Urban Radar*, published by CRC Press in 2011 and 2015, respectively.

Dr. Amin currently serves on the Editorial Board of the *IEEE Signal Processing Magazine*. He also serves on the Editorial Board of the *Signal Processing* journal. He was a Plenary Speaker at ISSPIT-2003, ICASSP-2010, ACES-2013, IET-2013, EUSIPCO-2013, STATOS-2013, CAMSAP-2013 and RADAR-2014. Dr. Amin was the Special Session Co-Chair of the 2008 IEEE International Conference on Acoustics, Speech, and Signal Processing; the Technical Program Chair of the 2nd IEEE International Symposium on Signal Processing and Information Technology, 2002; the General and Organization Chair of both the IEEE Workshop on Statistical Signal and Array Processing, 2000 and the IEEE International Symposium on Time- Frequency and Time-Scale Analysis, 1994. He was an Associate Editor of the *IEEE Transactions on Signal Processing* during 1996–1998; a member of the IEEE Signal Processing Society Technical Committee on Signal Processing for Communications during 1998–2002; a Member of the IEEE Signal Processing Society Technical Committee on Statistical Signal and Array Processing during 1995–1997. Dr. Amin was the Guest Editor of the *Journal of Franklin Institute* September-2008 Special Issue on Advances in Indoor Radar Imaging; a Guest Editor of the *IEEE Transactions on Geoscience and Remote Sensing* May-2009 Special Issue on Remote Sensing of Building Interior; a Guest Editor of the *IET Signal Processing* December-2009 Special Issue on Time- Frequency Approach to Radar Detection, Imaging, and Classification; a Guest Editor of the *IEEE Signal Processing Magazine* November-2013 and July- 2014 Special Issues on Time-frequency Analysis and Applications and Recent Advances in Synthetic Aperture Radar Imaging; and a Guest Editor of the *EURASIP Journal on Advances in Signal Processing* Special Issue on Sparse Sensing in Radar and Sonar Signal Processing.